Published in final edited form as:

J Alzheimers Dis. 2010 ; 19(1): 79–95. doi:10.3233/JAD-2010-1206.

INSULIN-DEGRADING ENZYME SORTING IN EXOSOMES: A SECRETORY PATHWAY FOR A KEY BRAIN Aβ-DEGRADING PROTEASE

Ayelén Bulloj[1,#], **María C. Leal**[1,#], **Huaxi Xu**[2], **Eduardo M. Castaño**[1], and **Laura Morelli**[1,*]

[1]Fundación Instituto Leloir. IIBBA- CONICET. Ave. Patricias Argentinas 435. Ciudad de Buenos Aires C1405BWE. Argentina.

[2]Center for Neuroscience and Aging, The Burnham Institute, La Jolla, California.

Abstract

The accumulation of Aβ peptides in the senile plaques is one of the hallmarks of Alzheimer disease (AD) progression. The endocytic pathway has been proposed as a major subcellular site for Aβ generation while the compartments in which Aβ-degrading proteases interact with Aβ are still elusive. It was suggested that extracellular Aβ degradation may take place by plasma-membrane associated proteases or by extracellular proteases, among which insulin-degrading enzyme (IDE) is the most relevant. However, the mechanisms of IDE secretion are poorly understood. In the present study we used N2a cells to explore if IDE is indeed released through exosomes and the effect of exosomes release on extracellular levels of Aβ. We demonstrated that proteolitically active plasma membrane associated-IDE is routed in living N2a cells to multivesicular bodies and subsequently, a major fraction is sorted to exosomes. We described that extracellular IDE levels decrease if the MVBs generation is interfered and may be positively modulated by exosomes release under stress-induced conditions. Our results reinforce the relevance of functional IDE in the catabolism of extracellular Aβ.

Keywords

multivesicular bodies; exosomes; amyloid β; peptide degradation; hypoxia; Alzheimer`s disease; IDE; calcium; VPS4; Rab11-GTPase; hypoxia

Introduction

The hypothesis that the progressive accumulation of aggregated forms of Aβ, as a consequence of a reduced Aβ turn-over in the human brain, may contribute to the development of AD [1, 2] was supported by experimental evidences showing that genetic targeted deletion of the brain peptidases involved in the catabolism of Aβ, neprylisin (NEP), endothelin converting enzyme (ECE) and insulin degrading enzyme (IDE), enhance Aβ accumulation in mice [3–5]. By contrast, over-expression of NEP or IDE in neurons of

[*]**Corresponding author:** Laura Morelli. Fundación Instituto Leloir. IIBBA-CONICET. Ave. Patricias Argentinas 435. Ciudad de Buenos Aires C1405BWE. Argentina. Phone: 54-11-5238-7500; Fax: 54-11-5238-7501; lmorelli@leloir.org.ar.
[#]A.B. and M.C.L. contributed equally to this work.

transgenic mice used as animal models of AD, showed reduction on the levels of soluble Aβ, prevention of amyloid plaque formation and extension of the life-span [6]. The endocytic pathway has been proposed as the main subcellular site for Aβ generation from its precursor protein by β and γ-secretases [7, 8] while the compartment in which Aβ-degrading proteases interact with Aβ is even now poorly described. It was suggested that plasma-membrane associated NEP, whose catalytic domain faces the extracellular space [9], is able to degrade either Aβ extracellularly or intracellularly after internalization of the complex NEP-Aβ in late endosomes while plasma-membrane associated IDE [10] and/or secreted IDE isoforms have a major role in the extracellular clearance of naturally secreted Aβ [11, 12]. In this scenario, IDE is one of the major secreted Aβ-degrading enzymes at neutral pH in rat and human brain however, its mechanisms of secretion are still elusive. Since IDE is mainly a cytosolic protein and lacks any secretory signal sequence, one should hypothesize that IDE is not released through the classical exocytic pathway. In this context, it was recently published that IDE is exported via an unconventional protein secretion pathway, different of microvesicle shedding, which remains to be elucidated [13]. In addition to shedding microvesicle, which are characterized by vesicles that buds directly from the plasma membrane into the extracellular space [14] alternative exocytic routes can be classified broadly into mechanisms whereby the protein is released into the external medium in free form or with vesicles [15]. These processes include direct traslocation through the plasma membrane mediated by transporters, incorporation into intracellular vesicles or autophagic internalization by an intracellular vesicle followed by fusion of the multi-vesiculated structures with the plasma membrane. Besides, it was extensively reported that in certain cell types, small local invaginations of the limiting membrane of endosomes generates multivesicular bodies (MVB) which may fuse with the cell surface, in an exocytic manner, resulting in the release of small vesicle of 50–90 nm diameter, contained in their lumen, namely exosomes [16]. Genetic screens in yeast have defined 17 different proteins that appear to play direct roles in MVB biogenesis (reviewed in [17]). All are required for vacuolar protein sorting (VPS), and are termed “class E” proteins because their deletion or inactivation induces formation of abnormally enlarged, highly tubulated endosomal membrane compartments that fail to mature normally into MVBs (known as “class E compartments”). Mechanisms involved in exosomes generation include cytosolic components (Tsg101, Alix) and the endosomal sorting complex (ESCRT) however, some proteins may be passively sorted into exosomes independently of the ESCRT machinery by partitioning into lipid microdomains [18]. Noteworthy, a pool of endogenous IDE localizes in detergent resistant domains in the plasma membrane [10] suggesting that this route may be used for IDE internalization and further secretion.

Over the past decade the potential sources of exosomes and their physiologic or pathologic relevant functions have significantly expanded [19]. In the context of Aβ generation and AD pathology, a recent report using mouse neuroblastoma N2a transfected cells over-expressing human Aβ peptide (N2aSW), suggested that Aβ produced in early endosomes is routed to MVBs and a minor fraction may be released in association with exosomes. In addition, exosomal proteins were found accumulated in senile plaques of AD patient brains [20] suggesting that MVBs may be involved in the neuropathogenic mechanisms of neurological diseases. In addition, it was also reported in exosomes derived from CHO cells over-

expressing wild type APP, the presence of α- and β-secretases (ADAM10 and BACE, respectively) and some components of the γ-secretase complex, namely presenilin 1 and presenilin 2. Because of the limited expression of some γ-secretase complex components, only a minor proportion of APP-CTFs then undergo γ-secretase cleavage to release Aβ or p3 fragments. This could be an explanation for the low levels of Aβ found in exosomes compared with other APP fragments [21].

Recent reports suggested that Rab11 GTPase participates in regulated exocytosis, promotes docking and fusion of MVBs favoring the shedding of vesicles into the extracellular media via fusion of MVBs with the plasma membrane [22]. However, overexpression of Rab11 or constitutively active Rab11 does not affect APP processing in HEK293 cells [23] .

A wide variety of stress signals could stimulate exosomes secretion including genotoxic stress, hypoperfusion (hypoxia) or the expression of activated oncogenes [24–26]. Interestingly, hypoxia was suggested to be linked with AD pathogenesis [27] since the metabolism of the Aβ is affected as a consequence of its over-production mediated by increased BACE expression [28] and γ-secretase activity [29]. This mechanism was considered part of the acute adaptive response of the brain to hypoxia [30] to restrict the progression of neurodegeneration.

In this study we were able to partially uncover the pathway of endogenous IDE secretion in N2a cells and the effect of exosomes-containing IDE release on extracellular Aβ levels. We demonstrated that proteolitically active plasma membrane associated-IDE is routed to MVBs and subsequently sorted to exosomes. We described that in N2aSW cells extracellular levels of Aβ are partially dependent on exosomes release. We showed that if MVBs formation is inhibited, by transfection with a VPS4A dominant negative mutant (E228Q), IDE secretion decreases and if exosomes release is favored, by Rab11 over expression or hypoxia, extracellular IDE levels increase. Our data reinforce the relevance of functional extracellular IDE in the catabolism of Aβ.

Materials and Methods

Reagents

Cell culture medium and fetal bovine serum (FBS) were obtained from Gibco. Monensin (MON), Brefeldin A, EGTA, Fura2-AM, acetylthiocholine, 5,5′-dithiobis(2-nitrobenzoic acid) and mono-dansyl cadaverine were from Sigma. N-(lissamine rhodamine B sulfonyl)-phosphatidylethanolamine (N-Rh-PE) was obtained from Avanti Polar Lipids, Inc. (Birmingham, AL). Ionophore A23187 was purchased from Molecular Probes.

Cell cultures and treatments

Mouse neuroblastoma N2a cells were cultured at 37°C in 50% DMEM/50% Opti-MEM supplemented with 5% fetal bovine serum (FBS) and antibiotics. N2aSW (N2a cells stably expressing human APP Swedish mutation [31]) were transfected with different construct cloned into the vector pEGFP-C1 (Clontech) such as: 1) cDNA of VPS4 dominant negative mutant (E228Q), kindly provided by Dr. Wesley Sundquist (Indiana University-USA) and 2) Rab11 wild type (Rab11WT) or its dominant negative mutant S25N (Rab11S25N), a

generous gift from Dr. Teresa Damiani (Universidad Nacional de Cuyo-Argentina) and cultured in N2a culture media supplemented with 400 Pg/ml of G418 (Sigma). Hypoxia was established by incubating cells overnight in a hypoxic chamber (StemCell Technologies Inc.) at 37°C and 5 % $C0_2$/ 0.1% O_2. To test cytotoxicity MTT (Sigma) cell proliferation and LDH assay (Promega) were performed.

Antibodies

BC2 rabbit polyclonal and 1C1 and 3A2 (isotype IgG1) monoclonal antibodies anti-IDE were generated in our laboratory as previously described [32, 33]. Anti-APP 4G8 and 6E10 monoclonal antibodies were purchased from Signet. Anti-APP C-terminal (AB5352) was from Chemicon International. Anti-flotillin and anti-Bip monoclonal antibodies were from BD Transduction Laboratories (San Jose, CA). Rabbit polyclonal 716 raised against synthetic peptides corresponding to residues 62–93 of Nicastrin [34] was a generous gift of Dr. Gopal Thinakaran (University of Chicago). Anti-Hsp/Hsc70 monoclonal antibody was obtained from Stressgen. Anti-TfR polyclonal CD71 SC9099 was purchase from Santa Cruz. We obtained monoclonal antibodies against lysobiophosphatidic acid (LBPA) (6C4) from Echelon Biosciences Inc. (Salt Lake City, UT).

Metabolic labeling and IDE pulse chase

N2aSW cells were incubated at 37 °C for 30 minutes in methionine-depleted medium (Invitrogen) and then pulse-labeled with 300 μCi/ml [35S]methionine (GE Biosciences) for 30 minutes at 37°C. After that, the radiolabeled medium was removed and replaced by fresh one. For MON or brefeldin (BFA) treatment, cells were preincubated with 7 μM MON or 18 μM BFA for 4 h before the labeling. BFA and MON were also added during the labeling and chase. After 2 h of chase conditioned medium was recovered and then IDE immunoprecipitated by using 1C1/3A2 monoclonal antibodies and analyzed by SDS-PAGE and autoradiography [10]. As a positive control of a protein released by the classical pathway we immunoprecipitated sαAPP with 6E10 monoclonal antibody following a previous report [35]. To determine whether the release of IDE is mediated by exocytosis, we examined the effect of low temperature, a classical blocker of vesicular exocytosis [36]. Cells were incubated for 3 hr at 18°C as previously described [36] and IDE detected in the supernatant as explained above.

Measurement of Intracellular Calcium Concentration

Cells plated in 24-well dishes (1×10^6 cells) were incubated in PBS/25 mM $CaCl_2$ in the presence or absence of 7 μM MON, 1.5 mM EGTA or 7 μM MON/1.5 mM EGTA for 30 minutes at room temperature (RT). Then 5 μM Fura2-AM (dissolved in 30 mM buffer Ca^{2+} free-Tris-HCl pH 7.4) supplemented with 1 mM digitonin was added for 30 minutes at RT protected from light. After incubation cells were washed to remove the extracellular dye and resuspended in water/10 mM digitonin to facilitate cellular lysis. Changes in fluorescence from each lysate were measured in an Aminco Bowman spectrofluorometer set as follow: λ excitation: 350/380 nm; λ emission: 510 nm. Data were analyzed using AB2 version 5,31 software.

MVBs labeling and IDE live staining immunofluorescence

To assess the presence of MVBs in N2a cells the fluorescent phospholipid analog N-Rh-PE, an useful marker for studying membrane traffic during endocytosis [37], was inserted into the plasma membrane as described previously [38]. Briefly, an appropriate amount of the lipid, stored in chloroform/methanol (2:1), was dried under nitrogen and subsequently solubilized in absolute ethanol. This ethanolic solution was injected with a Hamilton syringe into serum-free RPMI culture medium (<1%, v/v) while vigorously vortexing. The mixture was then added to the cells, which were incubated for 1 hour at 4 °C. After this incubation, the medium was discarded, and cells extensively washed with cold PBS to remove excess of unbound lipid. Slides were then incubated for 3 hours at 37 °C to allow internalization of the N-Rh-PE and its traffic to late endosome. In order to perform a co-localization with a specific maker of late endosomes, cells were then fixed with 3 % PFA, washed, treated with 50 mM NH_4CL, blocked with PBS-0.1 % BSA and incubated for 30 minutes with anti-LBPA monoclonal antibodies (6C4) in the presence of 0.05 % saponin as previously described [39] After that, coverslips were washed, incubated with Cy2-conjugated anti-mouse for 30 minutes, washed with PBS and mounted for confocal microscopy. To assess if IDE localizes in MVBs and taking into account that anti-LBPA (6C4) and anti-IDE (1C1/3A2) are monoclonal antibodies, living N2a cells were double-labeled with the N-Rh-PE and 1C1/3A2. For this aim, cells were incubated for 1 hour at 4°C with a mixture of N-Rh-PE and 1C1/3A2 (1μg/μl) to let insertion of the lipid to the plasma membrane and binding of anti-IDE to plasma membrane-associated IDE. Then, cells were washed and probed with Cy2-conjugated anti-mouse for 1 hour at 4°C. After washing with cold PBS, cells were incubated in Optimem for 3 hours at 37 °C as described above in the presence or absence of 7 μM MON, 1.5 mM EGTA or 1 μM A23187. Alternatively, for autophagosome labeling cells were incubated with 50μM mono-dansyl cadaverine in serum free media for ten minutes. In all cases, samples were fixed with 3 % PFA, mounted and the analysis of slides was performed by laser scanning confocal microscopy imaging on a Zeiss LSM5 Pascal or a Zeiss LSM5 Meta model 510 microscopes, according to the type of experiments, using a three-frame filter and a Zeiss LSM5 image examiner.

Exosomes Isolation

For western blot, electronmicroscopy and immunogold techniques, exosomes were isolated from 10 ml culture supernatants of N2a confluent cells grown for 12 hours. The supernatants were subjected to one centrifugation at 800 x g for 10 minutes to eliminate cells and subsequently were centrifuged at 12,000 x g for 30 minutes to remove the cellular debris, the pellet was referred as P2. Exosomes were separated from the supernatant by ultracentifugation at 100,000 x g for 2 hours. The pellet of the last centrifugation containing exosomes, referred as P3, was resuspended in 50 μl of PBS for further characterization. Exosomes were subjected to electrophoresis on 7.5 % SDS-Tris-Tricine polyacrylamide minigels, transferred to polyvinylidene fluoride (PVDF)-membranes (GE Healthcare) and membranes probed with the primary antibodies anti-flotillin, anti-Bip, anti-Nic and anti-IDE, respectively followed by horse radish peroxidase (HRP)-conjugated anti-gamma globulin (GE Healthcare). For visualization, blots were incubated with ECL Plus (GE Healthcare), scanned in a STORM 840 and processed using the computer software ImageQuant (GE Healthcare).

Immunoelectron Microscopy

Exosomes were fixed with paraformaldehyde 4% (1:1), applied to Formvar-carbon-coated EM grids (200 mesh) and negatively stained with 0.5 % uranyl acetate. For immunogold labeling, after fixation, grids were blocked with 0.05 M glycine/1% BSA and incubated with primary antibody at 0.5 μg/μl in PBS/0.02 %Triton-X 100/1 % BSA for 45 minutes. After washing, grids were incubated with goat anti-rabbit and/or goat anti-mouse conjugated with gold particles of 6 or 15 nm, respectively (Electron Microscopy Sciences). After fixing with 2 % glutaraldehide samples were negative stained with 0.5 % uranile acatate. Micrographs were taken under low-dose conditions with a JEOL 1200 EX II. The electronic photomicrograhs were obtained by using standard photographic and darkroom procedures.

Proteolysis Experiments

Purified exosomes from 25 ml of conditioned medium were centrifuged, the pellet resuspended in 20 μl of PBS and split into 2 tubes containing 10 mM EDTA in the presence or absence of 7 mM proteinase K (PK). Suspensions were incubated at 37°C for 30 minutes, then solubilized in Laemmli buffer and processed for western blotting as described above, using anti-IDE and anti-Hsp/Hsc70 primary antibodies.

IDE activity assay

Aliquots of 50 μl of exosomes isolated from 10 ml conditionated media were resuspended and sonicated in 0.1 M phosphate, pH 7 containing protease inhibitors PMSF, leupeptin, pepstatin, aprotinin, thiorphan and phosphoramidon with or without EDTA (5mM) and 1,10-phenanthroline (1mM). Homogenates were incubated with 35.000 cpm of ^{125}I-insulin, specific activity of 300 μCi/μg, for 3 hours and the degradation of radiolabeled substrate was analyzed by SDS-PAGE followed by exposure to a GP PhosphorImage screen (GE Healthcare), scanned in a STORM 840 and processed using the computer software ImageQuant (GE Healthcare).

Acetylcholinesterase (AChE) activity assay

The quantification of released exosomes was done by measuring the activity of AChE, as previously described [38]. Briefly, 20 μl of the exosome fraction isolated from 10 ml culture media were suspended in 100 μl of phosphate buffer and incubated with 1.25 mM acetylthiocholine and 0.1 mM 5,5′-dithiobis(2-nitrobenzoic acid) in a final volume of 300 μl The incubation was carried out in 96-wells plates at 37 °C, and the change in absorbance at 412 nm was monitored in a microplate reader (Bio-Rad 500) every 30 minutes up to 120 minutes for each experimental condition. The data represent the enzymatic activity in arbitrary units at 100 minutes of incubation as compared to control.

Quantification of endogenous Aβ

N2aSW cells were exposed or not to hypoxia in the presence of protease inhibitors PMSF (10 mM), leupeptin (20 μM), aprotinin (20 μM), thiorphan and phosphoramidon (50 μM). Aβ40 levels were quantified in the supernatants after 12 and 24 hours post-treatment by using a commercially available ELISA kit (BetaMark, Covance) following the manufacturer's instructions.

Quantitative Real-Time Polymerase Chain Reaction (RT-PCR)

Total RNA was extracted using RNasy Mini kit (Qiagen). SuperScript II Reverse transcriptase (Invitrogen) was used to synthesize first strand cDNA from samples with an equal amount of RNA, according to the manufacturer's instruction. Synthesized cDNAs were amplified using SYBR (R) GREEN I NUCLEIC A (Invitrogen) and Mx3005PCycler from Stratagene; data were analyzed using MxPRO-Mx3005P software. Primers used for BACE1 amplification were: BACE1–5, 5′-GATGGTGGACAACCTGAG-3′ and BACE1–3, 5′- CTGGTAGTAGCGATGCAG-3′. Primers used for TATA-Binding-Protein (TBP) amplification were: TBP-5, 5′-ACCGTGAATCTTGGCTGTAA −3′ and TBP-3, 5′-CCGTGGCTCTCTTATTCTCA −3′. BACE1 mRNA levels were normalized by TBP levels. Two independent experiments were performed, and statistical analysis was carried out using the Student's t test.

Image and Statistical analysis

Image analysis was performed in representative cells by counting single and double-stained vesicles with the "Manual Tag" tool of the Image ProPlus software (Media Cybernetics, Silver Springs, MD). Quantitative data were analyzed by one-way ANOVA with a post-hoc Tukey's test or two-tailed Student's t-test to treated and untreated cells using GraphPad Prism 3.0 software. Results were represented as means ± S.E.M. of at least 3 independent experiments performed in duplicate. p values lower than 0.05 were considered statistically significant.

Results

IDE release is not impaired by inhibition of the classical secretory pathway

To gain insight into the mechanism of IDE secretion N2aSW cells were metabolically labeled with L[^{35}S]methionine and then treated with monensin (MON) or brefeldin A (BFA) to interfere the trafficking by perturbing the ER or Golgi transport, respectively. We confirmed that these compounds produced no significant cytotoxic effects at the concentrations tested, as judged by quantification of MTT and LDH (data not shown). IDE was immunoprecipitated from the conditioned media by using a mix of anti-IDE monoclonal antibodies (1C1 and 3A2) and analyzed by SDS-PAGE and autoradiography (Fig. 1A, upper panel). As expected from the analysis of IDE primary sequence, we did not detect any significant reduction on extracellular levels of IDE after ER-Golgi disruption. Moreover, a remarkable 2.7-fold increase of IDE release was observed in cells incubated with MON compared to control (referred as 100 % of total secreted IDE) while a drastic abrogation of IDE secretion (less than 1 %) was detected in low-temperature (18 oC) incubated cells (Fig. 1A, lower panel). Released IDE was undetectable in the extracellular media of MON-treated cells incubated at 18 oC indicating that MON effect is not by leakage of the protein outside the cell due to potential toxicity of the drug (not shown). As expected, the secretion of soluble αAPP (sαAPP) was almost abolished at low temperature, as previously described [35], and in the presence of MON or BFA (Fig. 1A, upper panel) in accordance to a classical ER-Golgi dependent transported protein. These results suggested that IDE secretion may be mediated by an alternative exocytic route. Since it is known that MON induces Ca^{2+} entry and vesicle release [38, 40] we tested if MON used at the concentration previously assessed

increased Ca^{2+} intracellular levels. Therefore, we loaded N2a cells with Fura-2-AM and measured the ratio in the fluorescence at 350/385 nm. Our results showed that the Ca^{2+} rise induced by MON (1.78 ± 0.36 vs. 1.17 ± 0.12; $p<0.05$) was abolished by the previous addition of Ca^{2+} chelator EGTA (1.17 ± 0.12 vs. 1.18 ± 0.02; $p>0.05$) (Fig. 1B). These results suggest that IDE secretion may be mediated by a Ca^{2+} dependent vesicular transport. It has been shown by electron microscopy that treatment of cells with MON causes the formation of dilated MVBs [41]. To determine if N2a cells generate MVBs we performed immunofluorescence in N2a cells incubated with anti-LBPA (6C4), a well characterized marker protein for MVBs, and the fluorescent lipid analog N-Rh-PE. This strategy was used to validate the lipid staining as a MVBs marker as it is shown in Fig 2 (panels a–c). To identify if MVBs contain IDE, we performed immunofluorescence in N2a cells incubated with a mixture of the fluorescent lipid analog N-Rh-PE and 1C1 (anti-IDE monoclonal antibody). As it is shown in Fig. 2 (panels e–g) the MVBs labeled by the fluorescent lipid contain IDE.

Monensin and intracellular calcium levels induce the formation of large MVBs containing IDE

To assess if the amount of IDE in MVBs may be modulated by intracellular calcium levels, we performed immunofluorescence in N2a cells incubated with a mixture of the fluorescent lipid analog N-Rh-PE and 1C1 (anti-IDE monoclonal antibody) in the absence or presence of 7 μM MON. As it is shown in Fig. 3, MON caused the formation of large MVBs labeled by the fluorescent lipid in which IDE co-localized, suggesting that late endosomes may take part on the release of IDE into the extracellular environment upon exocytic fusion of multivesicular endosomes with the cell surface. Similar results were obtained after incubation with the Ca^{2+} ionophore (A23187) under experimental conditions that did not affect viability, as judged by quantification of MTT and LDH (data not shown) reinforcing the role of intracellular Ca^{2+} on IDE release. Moreover, addition of EGTA prevented MVBs enlargement. These results show that IDE localizes in MVBs.

IDE is released in association with exosomes

Because MVBs are precursors of exosomes we investigated if IDE was present in these vesicles. We followed the most common, simple and reliable method for exosomes purification from cell culture supernatants based on differential ultracentrifugation [42] and applied western blot and electron microscopy for characterizing and assessing the purity of the isolated vesicles. The exosomal fraction (pellet after 100,000 xg centrifugation step, namely P3) was qualitatively different from the previous fraction (pellet after 12,000 xg centrifugation step, namely P2) in the immunoreactivity assessed by western blot for IDE; flotillin-1, a protein that is abundant in exosomes [43] due to its raft association; Bip (an ER resident protein) and Nicastrin (a protein enriched in Golgi and plasma membrane) arguing against the possibility that the membranes harvested in P3 were cellular debris (Fig. 4A). Electron microscopic analysis of whole-mount fraction P3 revealed *cup-shaped* membrane vesicles mostly of 50–90 nm compatible with the typical profile and size of exosomes and fewer smaller (10 to 20 nm) ones as a result of morphological changes due to chemical fixation and contrasting with uranyl acetate as previously suggested [42] (Fig. 4B). Moreover, immunogold labeling of whole-mount exosomes with anti-transferrin receptor

(Fig. 4B inset, white arrow), that has been reported to be associated to exosomes in EM experiments [43], and anti-IDE (Fig. 4B inset, black arrow) showed co- localization of both proteins in these vesicles. To determine the topology of endogenous IDE in exosomes we used limited proteolysis of isolated exosomes with proteinase K (PK). Equivalent un-treated (−) and treated (+) fractions were analyzed for the presence of IDE, and Hsp/Hsc70 (Fig. 4C). After PK incubation, IDE and Hsp70 (72 kDa), the most strongly heat inducible form which is expressed on the surface of certain cells [44] were completely degraded while Hsc70 also known as p73 (70 kDa), a conventional cytoplasmic protein [45] remained intact suggesting that intraluminal exosomal proteins were not affected by the PK treatment and supporting that exosome-associated IDE is facing the extracellular space in accordance with its plasma membrane localization [10, 46].

To address the quantitative relevance of exosomes on IDE secretion conditioned media was split in 2 batches, one was untreated and used as positive (+) control for the presence of exosomes and the other one was subjected to the protocol for exosome isolation (as described above). The supernatant after 100.000 xg step was depleted of exosomes and referred as (−). IDE was immunoprecipitated from both conditioned media and detected by SDS-PAGE and western blot. As it is shown in Fig. 4D (upper panel) IDE levels detected in the exosomes-depleted supernatant were 56 ± 11 % lower as compared with control, indicating that exosomes is a relevant pathway for IDE secretion (Fig. 4D, lower panel).

Exosome-associated IDE is proteolytically active

It was suggested that exosomes may be one of the mechanisms involved in the elimination of obsolete proteins from the plasma membrane of reticulocytes [47]. To assess if N2a cells use exosomes to remove proteolytic inactive plasma membrane IDE we sonicated the exosome fraction and we performed a degradation assay using ^{125}I-insulin in the presence or absence of EDTA and 1.10 phenantroline, known to inhibit Zn-metalloproteases. As it is shown in a representative phosphorimage scan (Fig 5, upper panel) exosomes-associated IDE degraded ^{125}I-insulin in the absence of protease inhibitors. Semi-quantitative analysis of the data (Fig. 5, lower panel) showed a mean degradation value of 48.7 ± 10.9 % (n=2, $p<0.05$) in 3 hours as compared to inhibited IDE indicating that IDE in exosomes is not aggregated, it is natively folded and retains its catalytic activity. In addition, this result rules out the unlikely possibility that aggregated IDE accounted for the positive Western blot in fraction P3 shown in figure 4A.

VPS4 modulates the exosomal pathway, IDE release and the catabolism of endogenous Aβ

As both endocytic and biosynthetic traffic to the lysosome/vacuole proceeds via the MVBs, and taking into account that loss of VPS4 function in mammalian cells disrupts MVBs sorting, we assessed the impact of a dominant negative form of VPS4 (E228Q), which lacks ATPase activity, on IDE release. Expression of the transfected proteins was visualized by fluorescence microscopy. As previously reported, transient expression of the dominant negative VPS4 in cultured cells led to unusually enlarged aberrant endosomes. By contrast, mock-transfected cells showed a homogeneous cytoplasmic and nuclear green staining distributed in a non-vesiculated pattern (Fig. 6A). To assess if VPS4-E228Q affected exosomes release we determined the acethyl cholinesterase (AChE) activity. Our results

showed (Fig. 6B) a decrement of 13.9 % of released AChE (in arbitrary units) in VPS4-dominant negative as compared to mock-transfected N2aSW cells (100.0 ± 0.58 vs. 86.10 ± 2.70; n=3; $p<0.05$). By contrast to secreted APP, IDE immunoreactivity was decreased in the conditioned supernatant from VPS4-E228Q transfected cells (Fig 6C, upper panel) as compared to control. The semi-quantitative analysis (Fig. 6C, lower panel) showed statistical significant decrements in IDE/APP secretion (in arbitrary units) as compared to control (1.95 ± 0.27 vs. 2.48 ± 0.30; n=3, $p<0.05$) reinforcing the concept that IDE release may be partially mediated by a VPS4-dependent exosomal mechanism. To determine the impact of reduced-IDE secretion on Aβ catabolism, 16 h after transfection the levels of extracellular Aβ were determined by ELISA. As it is shown in Fig. 6D, an increment of 42,95 % in Aβ levels was detected in VPS4-E228Q as compared to empty vector transfected cells (n= 3). In addition, we confirmed by westernblot and by quantitative real-time PCR that APP-CTF/tubulin levels (Fig. 6 E, upper panel) and mRNA transcripts of BACE/TBP (Fig. 6E, lower panel), respectively, were unchanged after VPS4-dominant negative expression. This set of experiments raises the possibility that a decrease in the release of exosome-associated IDE accounted for a decrease in the rate of degradation of extracellular Aβ.

Rab11 modulates the exosomal pathway and IDE release in N2a cells

To further characterize IDE release N2aSW cells were transfected with pEGFP-Rab11 wild type (WT), pEGFP-Rab11S25N (GDP bound inactive mutant) and the empty vector p-EGFP, respectively. Expression of the transfected proteins was visualized by fluorescence microscopy (not shown). To assess the amount of exosomes released in each experimental condition we determined the acethyl cholinesterase (AChE) activity. Our results showed (Fig. 7A), in agreements with previous reports, increments in the amount (in arbitrary units, A.U.) of released AChE by Rab11WT transfected as compared with control N2aSW cells (4.50 ± 0.10 vs. 1.05 ± 0.05; n=2, $p<0.05$). However, Rab11S25N did not reduce exosome release as compared to p-EGFP control cells (0.90 ± 0.01 vs. 1.05 ± 0.05; n=2, $p<0.05$), suggesting that in N2aSW was inactive but it did not behave as a dominant negative probably due to the effect exerted in this mechanism by another endogenous Rab. IDE immunoreactivity was increased in exosomes isolated from Rab11WT-transfected cells (Fig 7B, upper panel) and the semi-quantitative analysis (Fig. 7B, lower panel) showed statistical significant increments as compared to control (1.80 ± 0.10 vs. 1.20 ± 0.10; n=2, $p<0.05$) suggesting that IDE secretion is mediated by a Rab11-dependent exosomal release. Differences in the relative increases in AChE and IDE secretion may be due to several factors including the dynamic range of the techniques and/or a difference in the number of molecules of AChE or IDE per exosomal vesicle.

Exosomes-mediated IDE release impact on the catabolism of Aβ

Using N2aSW cells two different approaches were experimentally addressed. First, cells were transfected with pEGFP or Rab11WT, respectively, and after 24 h the levels of extracellular Aβ were determined by ELISA. As it is shown in Fig. 7C, a significant decrease in Aβ levels was detected in Rab11WT as compared to empty vector (807.86 ± 66.23 pg/mg vs. 437.68 ± 32.94 pg/mg; n=3; $p< 0.05$) raising the possibility that an increase in the release of exosome-associated IDE accounted for an increase in the rate of

degradation of extracellular Aβ. Second, taking into account that hypoxia promotes exosomes release [25] and Aβ production [29] we wondered if the steady-state levels of Aβ were altered after exposing cells to low oxygen tension. As it is shown in Fig. 8A large MVBs containing IDE were obtained when cells were exposed to hypoxia as compared with normoxia (size particle 9.9 ± 0.9 vs. 4.6 ± 0.3 pixels/particle; n= 18 cells, $p<0.05$). To rule out that larger MVBs containing IDE were autophagic vacuoles we labeled cells with anti-IDE and mono-dansyl cadaverine. Analysis of the co-localization of the staining showed that IDE was not routed to the autophagic pathway under hypoxia (not shown). Next, we corroborated that hypoxia stimulated exosome release in N2aSW cells, as previously reported in ovarian carcinoma cells [25], by determination of the AChE activity (1.5 ± 0.2 vs. 4.6 ± 0.1, n=4, $p<0.001$) (Fig. 8B, left panel). This effect was confirmed by the increments on exosomal-Hsp70 immunoreactivity detected by western blot (Fig. 8B, upper right panel) (2.4 ± 0.05 vs. 3.5 ± 0.2; n=3, $p<0.05$). In addition, by quantitative real-time PCR, we confirmed that mRNA transcripts of BACE were increased after hypoxia (Fig. 9A) (1.1 ± 0.1 vs. 7.3 ± 1.3; n=2, $p<0.05$) in accordance with increments in membrane-bound APP-CTF fragments determined by western blot (1.02 ± 0.03 vs. 1.53 ± 0.1; n=2, $p<0.05$ (Fig. 9B) as previously reported [28]. Both effects should be reflected in over-production of endogenous Aβ and increased extracellular levels of the peptide. However, no significant differences were detected on the levels of extracellular Aβ between normoxia and hypoxia (Fig. 9C) (454.42 ± 52.03 pg/mg vs. 475.01 ± 120.26 pg/mg total protein; n=4, p=0.88). Subsequently, we immunoprecipitated IDE from the conditioned media and we confirmed increased levels of IDE in hypoxia as compared to normoxia (1.07 ± 0.04 vs. 1.8 ± 0.03; n=3, $p<0.05$) (Fig 9D) strongly supporting that promotion of Aβ production, under hypoxia, may be balanced by the over-expression of IDE in the extracellular space.

Discussion

Our metabolic labeling and pulse-chase experiments of endogenous IDE in the presence of inhibitors of the ER-Golgi transport strongly support that IDE is not secreted through the classical secretory pathway. These results concur with those recently published by Zhao et al. [13] using murine hepatocytes and Hela cells. However, in our experiments, MON and Ca^{2+} ionophore clearly stimulated IDE release. These discrepancies may be due to the different experimental approach. Zhao et al. co-transfected immortalized murine hepatocytes with human IDE and human α1-antitrypsin, and evaluated the release of over-expressed IDE and over-expressed α1-antitrypsin by western blot of a 100-fold concentrated supernatants. In turn, we studied the release of endogenous IDE from N2a cells and used endogenous sAPP as control of a protein secreted by the classical pathway by pulse-chase and immunoprecipitation of IDE from conditioned supernatants with specific anti-IDE monoclonal antibodies. In addition, cytotoxicity of 50 μM MON and 10 μM A23187 reported by Zhao et al. may be due to a 7-fold and 10-fold increase concentration, respectively, as compared to our experimental conditions. Taking into account that incubation of cells at 18 °C abolished the presence of extracellular IDE and Ca^{2+} promote its secretion, we hypothesized that a vesicle–mediated transport [35] was involved in the liberation of IDE into the extracellular environment.

Taken together, our results of *in vivo* immunofluorescence, pharmacological treatments, electron microscopy and cell transfection with VPS4 dominant negative and Rab11 GTPase, strongly suggest that a substantial population of IDE molecules are secreted in association with exosomes. Our estimation is that at least 50 % of extracellular IDE is secreted by this way, since it is known that proteins may be released from exosomes once these vesicles are in the extracellular compartment [48, 49]. An intriguing aspect of the present work is how IDE is targeted to exosomes. MVBs, the organelles from which exosomes are derived, are generated from the fusion of early endosomes and have a well established role in the degradation of proteins internalized from the cell surface via fusion with lysosomes. However, in addition to fusion with lysosomes, MVBs are able to undergo exocytic fusion with the plasma membrane and release exosomes. IDE is localized on the cell surface with an extracellular topology [10, 46]. While the exact mechanisms underlying IDE association with membranes remains to be elucidated, we demonstrated that a pool of endogenous IDE is routed from the plasma membrane in living N2a cells to MVBs by a Ca^{2+}-dependent mechanism and subsequently, a fraction of IDE is sorted to exosomes and released in a Rab11-dependent manner. Moreover, IDE secretion is significantly reduced after introduction of a dominant negative form of VPS4, a protein involved in MVBs generation. It is important to note that the role of Rab proteins in APP processing was extensively investigated, suggesting that Rab6, a Ras-superfamily member likely responsible for intra-Golgi routing, appears to be involved in APPα secretion without contributing to Aβ production [50] while Rab1B, which blocks early steps of endoplasmic reticulum to Golgi transport, drastically decreases the APPα secretion in HEK293 cells [51]. Our results, in agreement to previous reports [23] suggest that Rab 11 in N2a cells does not significantly alter APP processing. However, our study hint that Rab11 in neuroblastoma cells might drive exosomes release preventing fusion of MVBs with lysosomes, as previously reported in an erythroleukemia cell line of human origin [22] and support the concept formerly described [52] that this mechanism is likely to be critical in neuronal cells determining the secretory fate of a transport vesicle.

Although in this work we did not demonstrate that cytosolic IDE translocates to the lumen along the endocytic pathway we cannot rule out this possibility to explain the finding of IDE on the extracellular side of the plasma membrane and exosomes. Alternatively, it may be also possible that cytosolic IDE translocates to endosomes, as previously suggested [53], and further routed to the degradation pathway or that portions of cytosol containing IDE may be sequestered by the phagophore and incorporated into the autophagolysosome which may fuse with MVBs [54] precluding in these cases the detection of IDE in the lumen of exosomes.

We describe that exosomes contributed to the release of IDE from N2a cells in both the basal and stress-induced state. Specifically, we showed that hypoxia enhanced the exosome secretory rate, as previously reported in a different cell line [25], and increased the extracellular levels of IDE suggesting that both events are physiologically linked.

It was previously reported that hypoxia promotes Aβ over-production by enhancing BACE and γ-secretases activities on the Aβ precursor protein [28, 29]. In our experiments we showed increased exosomal release and increments in the exosomal IDE-associated levels,

which means that under hypoxic conditions IDE is overexpressed and released by exosomes. *In silico* analysis of IDE promoter [55] showed hypoxia responsive elements (HRE) which may bind Hif-1α/β. In this regard, it is possible that short periods of hypoxia (2–8 h at 1 % O_2) as described in the previous reports [29] are not enough to promote IDE transcription and/or exosomes release and this may explain Aβ increments. This hypothesis is supported by recent experimental evidences showing in NB7 cells, increments on mRNA transcripts of neprilysin (NEP), another relevant Aβ degrading protease, after 24 h of incubation under reduced oxygen content to 2.5% [56]. The observation that the steady-state levels of extracellular Aβ were not significantly changed in cells exposed to low O_2 levels suggested that the increments on Aβ production were balanced by increasing the levels of either plasma membrane associated or extracellular Aβ-proteases. The hypoxia-mediated increase in exosomes release and extracellular IDE support the participation of IDE in this homeostatic mechanism.

Whether exosomes-associated IDE could play a role in the pathogenesis of AD is yet to be studied but the evidences that Aβ and IDE are present in plasma-membrane lipid rafts [10], are enriched in the amyloid plaques [57], are components of a stable complex in the brain [58] and are both detected in exosomes reinforce the hypothesis that the interaction of Aβ with IDE takes place in restricted compartments that require a proper sorting of the protease to regulate Aβ catabolism. Taking into account the recently reported evidences supporting the functional importance of lipidated APOE and extracellular IDE in the proteolytic degradation of soluble Aβ [11], the present study documents the first described pathway for IDE secretion. The fact that IDE faces the outer side of exosomes and plasma-membrane [10, 45], may be relevant to the interaction with lipidated APOE-Aβ complexes spread in the interstitial brain fluids facilitating the clearance of extracellular Aβ. Our data raise the possibility that the mis-sorting of IDE to exosomes may be a novel post-translational mechanism involved in a defective extracellular Aβ clearance. In this regard, it is important to note that abnormally large early endosomes, the precursors of MVBs, and lysosomes are detected in early stages of AD [59]. Under pathologic conditions, it is possible that the fusion of late endosomes/MVBs with autophagosomes, to further mature into lysosomes, is favored over the interaction of MVBs with the plasma membrane to release exosomes. In this context and taking into account our data, the secretion of extracellular IDE may be strongly impaired under such conditions.

In conclusion, here we have generated several experimental evidences showing an exosome-based mechanism in the targeting of IDE to the extracellular space of N2a cells. Besides its potential relevance for the degradation of extracellular Aβ, the presence of IDE in exosomes may have a number of still unexplored implications and is a challenge for future research.

Acknowledgments

This work was supported by grants from Agencia Nacional de Promoción Científica y Tecnológica ANPCyT (PICT 05-10599, PICT 05-38009) and Consejo Nacional de investigaciones Científicas y Técnicas CONICET (PIP 6164) to LM. Research reported in this publication was also supported by grants to H.X. from the National Institute of Health (R01NS046673 and R01AG030197).

References

1. Perez A, Morelli L, Cresto JC, Castano EM. Degradation of soluble amyloid beta-peptides 1–40, 1–42, and the Dutch variant 1–40Q by insulin degrading enzyme from Alzheimer disease and control brains. Neurochem Res. 2000; 25:247–255. [PubMed: 10786709]
2. Yasojima K, Akiyama H, McGeer EG, McGeer PL. Reduced neprilysin in high plaque areas of Alzheimer brain: a possible relationship to deficient degradation of beta-amyloid peptide. Neurosci Lett. 2001; 297:97–100. [PubMed: 11121879]
3. Iwata N, Tsubuki S, Takaki Y, Shirotani K, Lu B, Gerard NP, Gerard C, Hama E, Lee HJ, Saido TC. Metabolic regulation of brain Abeta by neprilysin. Science. 2001; 292:1550–1552. [PubMed: 11375493]
4. Eckman EA, Watson M, Marlow L, Sambamurti K, Eckman CB. Alzheimer's disease beta-amyloid peptide is increased in mice deficient in endothelin-converting enzyme. J Biol Chem. 2003; 278:2081–2084. [PubMed: 12464614]
5. Farris W, Mansourian S, Chang Y, Lindsley L, Eckman EA, Frosch MP, Eckman CB, Tanzi RE, Selkoe DJ, Guenette S. Insulin-degrading enzyme regulates the levels of insulin, amyloid beta-protein, and the beta-amyloid precursor protein intracellular domain in vivo. Proc Natl Acad Sci U S A. 2003; 100:4162–4167. [PubMed: 12634421]
6. Leissring MA, Farris W, Chang AY, Walsh DM, Wu X, Sun X, Frosch MP, Selkoe DJ. Enhanced proteolysis of beta-amyloid in APP transgenic mice prevents plaque formation, secondary pathology, and premature death. Neuron. 2003; 40:1087–1093. [PubMed: 14687544]
7. Koo EH, Squazzo SL. Evidence that production and release of amyloid beta-protein involves the endocytic pathway. J Biol Chem. 1994; 269:17386–17389. [PubMed: 8021238]
8. Perez RG, Soriano S, Hayes JD, Ostaszewski B, Xia W, Selkoe DJ, Chen X, Stokin GB, Koo EH. Mutagenesis identifies new signals for beta-amyloid precursor protein endocytosis, turnover, and the generation of secreted fragments, including Abeta42. J Biol Chem. 1999; 274:18851–18856. [PubMed: 10383380]
9. Devault A, Lazure C, Nault C, Le Moual H, Seidah NG, Chretien M, Kahn P, Powell J, Mallet J, Beaumont A, et al. Amino acid sequence of rabbit kidney neutral endopeptidase 24.11 (enkephalinase) deduced from a complementary DNA. Embo J. 1987; 6:1317–1322. [PubMed: 2440677]
10. Bulloj A, Leal MC, Surace EI, Zhang X, Xu H, Ledesma MD, Castano EM, Morelli L. Detergent resistant membrane-associated IDE in cultured cells and brain tissue: Relevance to Abeta and insulin degradation. Mol Neurodegener. 2008; 3:22. [PubMed: 19117523]
11. Jiang Q, Lee CY, Mandrekar S, Wilkinson B, Cramer P, Zelcer N, Mann K, Lamb B, Willson TM, Collins JL, Richardson JC, Smith JD, Comery TA, Riddell D, Holtzman DM, Tontonoz P, Landreth GE. ApoE promotes the proteolytic degradation of Abeta. Neuron. 2008; 58:681–693. [PubMed: 18549781]
12. Vekrellis K, Ye Z, Qiu WQ, Walsh D, Hartley D, Chesneau V, Rosner MR, Selkoe DJ. Neurons regulate extracellular levels of amyloid beta-protein via proteolysis by insulin-degrading enzyme. J Neurosci. 2000; 20:1657–1665. [PubMed: 10684867]
13. Zhao J, Li L, Leissring MA. Insulin-degrading enzyme is exported via an unconventional protein secretion pathway. Mol Neurodegener. 2009; 4:4. [PubMed: 19144176]
14. Cocucci E, Racchetti G, Meldolesi J. Shedding microvesicles: artefacts no more. Trends Cell Biol. 2009; 19:43–51. [PubMed: 19144520]
15. Hughes RC. Secretion of the galectin family of mammalian carbohydrate-binding proteins. Biochem Biophys Acta. 1999; 1473:172–185. [PubMed: 10580137]
16. Thery C, Zitvogel L, Amigorena S. Exosomes: composition, biogenesis and function. Nat Rev Immunol. 2002; 2:569–579. [PubMed: 12154376]
17. Katzmann DJ, Odorizzi G, Emr SD. Receptor downregulation and multivesicular-body sorting. Nat Rev Mol Cell Biol. 2002; 3:893–905. [PubMed: 12461556]
18. Reggiori F, Pelham HR. Sorting of proteins into multivesicular bodies: ubiquitin-dependent and -independent targeting. Embo J. 2001; 20:5176–5186. [PubMed: 11566881]

19. Fevrier B, Raposo G. Exosomes: endosomal-derived vesicles shipping extracellular messages. Curr Opin Cell Biol. 2004; 16:415–421. [PubMed: 15261674]
20. Rajendran L, Honsho M, Zahn TR, Keller P, Geiger KD, Verkade P, Simons K. Alzheimer's disease beta-amyloid peptides are released in association with exosomes. Proc Natl Acad Sci U S A. 2006; 103:11172–11177. [PubMed: 16837572]
21. Sharples RA, Vella LJ, Nisbet RM, Naylor R, Perez K, Barnham KJ, Masters CL, Hill AF. Inhibition of γ-secretase causes increased secretion of amyloid precursor protein C-terminal fragments in association with exosomes. The FASEB J. 2008; 22:1469–1478.
22. Savina A, Fader CM, Damiani MT, Colombo MI. Rab11 promotes docking and fusion of multivesicular bodies in a calcium-dependent manner. Traffic. 2005; 6:131–143. [PubMed: 15634213]
23. Lopez-Perez E, Dumanchin C, Czech C, Campion D, Goud B, Pradier L, Frebourg T, Checler F. Overexpression of Rab11 or constitutively active Rab11 does not affect sAPPalpha and Abeta secretions by wild-type and Swedish mutated betaAPP-expressing HEK293 cells. Biochem Biophys Res Commun. 2000; 275:910–915. [PubMed: 10973821]
24. Yu X, Harris SL, Levine AJ. The regulation of exosome secretion: a novel function of the p53 protein. Cancer Res. 2006; 66:4795–4801. [PubMed: 16651434]
25. Gutwein P, Stoeck A, Riedle S, Gast D, Runz S, Condon TP, Marme A, Phong MC, Linderkamp O, Skorokhod A, Altevogt P. Cleavage of L1 in exosomes and apoptotic membrane vesicles released from ovarian carcinoma cells. Clin Cancer Res. 2005; 11:2492–2501. [PubMed: 15814625]
26. Amzallag N, Passer BJ, Allanic D, Segura E, Thery C, Goud B, Amson R, Telerman A. TSAP6 facilitates the secretion of translationally controlled tumor protein/histamine-releasing factor via a nonclassical pathway. J Biol Chem. 2004; 279:46104–46112. [PubMed: 15319436]
27. Di Legge S, Hachinski V. Prospects for prevention and treatment of vascular cognitive impairment. Curr Opin Investig Drugs. 2003; 4:1082–1087.
28. Sun X, He G, Qing H, Zhou W, Dobie F, Cai F, Staufenbiel M, Huang LE, Song W. Hypoxia facilitates Alzheimer's disease pathogenesis by up-regulating BACE1 gene expression. Proc Natl Acad Sci U S A. 2006; 103:18727–18732. [PubMed: 17121991]
29. Zhang X, Zhou K, Wang R, Cui J, Lipton SA, Liao FF, Xu H, Zhang YW. Hypoxia-inducible factor 1alpha (HIF-1alpha)-mediated hypoxia increases BACE1 expression and beta-amyloid generation. J Biol Chem . 2007; 282:10873–10880. [PubMed: 17303576]
30. Baiden-Amissah K, Joashi U, Blumberg R, Mehmet H, Edwards AD, Cox PM. Expression of amyloid precursor protein (beta-APP) in the neonatal brain following hypoxic ischaemic injury. Neuropathol Appl Neurobiol. 1998; 24:346–352. [PubMed: 9821164]
31. Thinakaran G, Teplow DB, Siman R, Greenberg B, Sisodia SS. Metabolism of the "Swedish" amyloid precursor protein variant in neuro2a (N2a) cells. Evidence that cleavage at the "beta-secretase" site occurs in the golgi apparatus. J Biol Chem. 1996; 271:9390–9397. [PubMed: 8621605]
32. Morelli L, Llovera RE, Mathov I, Lue LF, Frangione B, Ghiso J, Castano EM. Insulin-degrading enzyme in brain microvessels: proteolysis of amyloid [28] vasculotropic variants and reduced activity in cerebral amyloid angiopathy. J Biol Chem. 2004; 279:56004–56013. [PubMed: 15489232]
33. Leal MC, Dorfman VB, Gamba AF, Frangione B, Wisniewski T, Castano EM, Sigurdsson EM, Morelli L. Plaque-associated overexpression of insulin-degrading enzyme in the cerebral cortex of aged transgenic tg2576 mice with Alzheimer pathology. J Neuropathol Exp Neurol. 2006; 65:976–987. [PubMed: 17021402]
34. Leem JY, Vijayan S, Han P, Cai D, Machura M, Lopes KO, Veselits ML, Xu H, Thinakaran G. Presenilin 1 is required for maturation and cell surface accumulation of nicastrin. J Biol Chem. 2002; 277:19236–19240. [PubMed: 11943765]
35. Xu H, Sweeney D, Wang R, Thinakaran G, Lo ACY, Sisodia SS, Greengard P, Gandy S. Generation of Alzheimer β-amyloid protein in the trans-Golgi network in the apparent absence of vesicle formation. Proc Natl Acad Sci U S A. 1997; 94:3748–3752. [PubMed: 9108049]

36. Lee HJ, Patel S, Lee SJ. Intravesicular Localization and Exocytosis of α-Synuclein and its Aggregates. The Journal of Neuroscience. 2005; 25:6016–6024. [PubMed: 15976091]
37. Willem J, ter Beest M, Scherphof G, Hoekstra D. A non-exchangeable fluorescent phospholipid analog as a membrane traffic marker of the endocytic pathway. Eur J Cell Biol. 1990; 53:173–184. [PubMed: 2076704]
38. Savina A, Furlan M, Vidal M, Colombo MI. Exosome release is regulated by a calcium-dependent mechanism in K562 cells. J Biol Chem. 2003; 278:20083–20090. [PubMed: 12639953]
39. Kobayashi T, Startchev K, Whitney AJ, Gruenber. Localization of lysobisphosphatidic acid-rich membrane domains in late endosomes. J. Biol Chem. 2001; 382:483–485. [PubMed: 11347897]
40. Nassar-Gentina V, Rojas E, Luxoro M. Rise in cytoplasmic Ca2+ induced by monensin in bovine medullary chromaffin cells. Cell Calcium. 1994; 16:475–480. [PubMed: 7712541]
41. Stein BS, Bensch KG, Sussman HH. Complete inhibition of transferrin recycling by monensin in K562 cells. J Biol Chem. 1984; 259:14762–14772. [PubMed: 6094573]
42. Thery C, Amigorena S, Raposo G, Clayton A. Isolation and characterization of exosomes from cell culture supernatants and biological fluids. Curr Protoc Cell Biol Chapter. 2006; 3(Unit 3):22.
43. Raposo G, Nijman HW, Stoorvogel W, Liejendekker R, Harding CV, Melief CJ, Geuze HJ. B lymphocytes secrete antigen-presenting vesicles. J Exp Med. 1996; 183:1161–1172. [PubMed: 8642258]
44. Gross C, Koelch W, DeMaio A, Arispe N, Multhoff G. Cell surface-bound heat shock protein 70 (Hsp70) mediates perforin-independent apoptosis by specific binding and uptake of granzyme B. J Biol Chem. 2003; 278:41173–41181. [PubMed: 12874291]
45. Pelham HR. Speculations on the functions of the major heat shock and glucose-regulated proteins. Cell. 1986; 46:959–961. [PubMed: 2944601]
46. Li Q, Ali MA, Cohen JI. Insulin degrading enzyme is a cellular receptor mediating varicella-zoster virus infection and cell-to-cell spread. Cell. 2006; 127:305–316. [PubMed: 17055432]
47. Johnstone RM, Mathew A, Mason AB, Teng K. Exosome formation during maturation of mammalian and avian reticulocytes: evidence that exosome release is a major route for externalization of obsolete membrane proteins. J Cell Physiol. 1991; 147:27–36. [PubMed: 2037622]
48. Mehul B, Hughes RC. Plasma membrane targetting, vesicular budding and release of galectin 3 from the cytoplasm of mammalian cells during secretion. J Cell Sci . 1997; 110(Pt 10):1169–1178. [PubMed: 9191041]
49. Dennis EA. Diversity of group types, regulation, and function of phospholipase A2. J Biol Chem. 1994; 269:13057–13060. [PubMed: 8175726]
50. McConlogue L, Castellano F, deWit C, Schenk D, Maltese WA. Differential effects of a Rab6 mutant on secretory versus amyloidogenic processing of Alzheimer's beta-amyloid precursor protein. J Biol Chem. 1996; 271:1343–1348. [PubMed: 8576122]
51. Dugan JM, deWit C, McConlogue L, Maltese WA. The Ras-related GTP-binding protein, Rab1B, regulates early steps in exocytic transport and processing of beta-amyloid precursor protein. J Biol Chem. 1995; 270:10982–10989. [PubMed: 7738040]
52. Khvotchev MV, Ren M, Takamori S, Jahn R, Sudhof TC. Divergent functions of neuronal Rab11b in Ca2+-regulated versus constitutive exocytosis. J Neurosci. 2003; 23:10531–10539. [PubMed: 14627637]
53. Authier F, Cameron PH, Taupin V. Association of insulin-degrading enzyme with a 70 kDa cytosolic protein in hepatoma cells. Biochem J . 1996; 319(Pt 1):149–158. [PubMed: 8870662]
54. Fader CM, Sanchez D, Furlan M, Colombo MI. Induction of autophagy promotes fusion of multivesicular bodies with autophagic vacuoles in k562 cells. Traffic. 2008; 9:230–250. [PubMed: 17999726]
55. Farris W, Leissring MA, Hemming ML, Chang AY, Selkoe DJ. Alternative splicing of human insulin-degrading enzyme yields a novel isoform with a decreased ability to degrade insulin and amyloid beta-protein. Biochemistry. 2005; 44:6513–6525. [PubMed: 15850385]
56. Fisk L, Nalivaeva NN, Boyle JP, Peers CS, Turner AJ2. Effects of hypoxia and oxidative stress on expression of neprilysin in human neuroblastoma cells and rat cortical neurones and astrocytes. Neurochem Res. 2007; 32:1741–1748. [PubMed: 17486446]

57. Dorfman VB, Pasquini L, Riudavets M, López-Costa JJ, Villegas A, Troncoso JC, Lopera F, Castaño EM, Morelli L. Differential cerebral deposition of IDE and NEP in sporadic and familial Alzheimer's disease. Neurobiol Aging. 2008 Epub ahead of print.

58. Llovera RE, de Tullio M, Alonso LG, Leissring MA, Kaufman SB, Roher AE, de Prat G, Morelli L, Castano EM. The catalytic domain of insulin-degrading enzyme forms a denaturant-resistant complex with amyloid beta peptide: implications for Alzheimer disease pathogenesis. J Biol Chem. 2008; 283:17039–17048. [PubMed: 18411275]

59. Nixon RA. Autophagy, amyloidogenesis and Alzheimer disease. J Cell Sci. 2007; 120:4081–4091. [PubMed: 18032783]

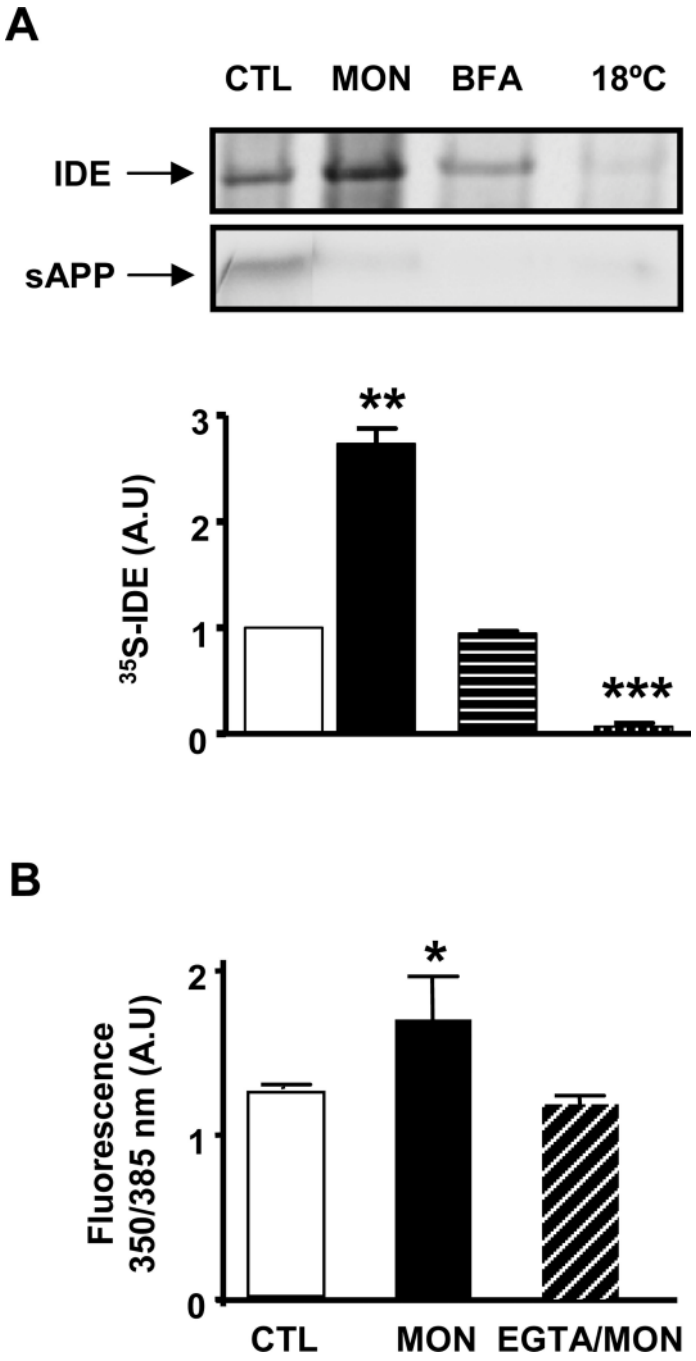

Fig. 1. IDE is not secreted by the classical ER-Golgi secretory pathway

A. Upper panel, representative phosphorimage scan of the immunoprecipitation of IDE and sαAPP from N2aSW cells metabolically labeled with 300 μCi of L[^{35}S]-methionine and treated with 7 μM MON or 18 μM BFA for 7 hours. IDE was immunoprecipitated by using 1C1/3A2 monoclonal antibodies. Immunoprecipitation of sαAPP with 6E10 was performed as a control for an ER-Golgi dependent transported protein. Lower panel, bars show the semi-quantitative analysis of IDE immunoreactivity expressed in arbitrary units (A.U.) in control and treated-cells. MON stimulates IDE release compared to control (CTL) (1 ± 0.2

vs. 2.7 ± 0.1; n=3; *p<0.05) while low temperatures (18°C) almost abolished IDE release (0.06 ± 0.03 vs. 1 ± 0.2; n=3; **p<0.0001). No significant differences were observed during BFA treatment as compared to control. **B**. Bars show the fluorescence in arbitrary units (A.U.) at 350/385 nm of N2a cells loaded with Fura-2-AM in the absence or presence of 7 μM MON or 7 μM MON/1.5 mM EGTA. Intracellular Ca^{2+} levels were significantly increased in MON treated cells as compared with CTL (*p<0.05)

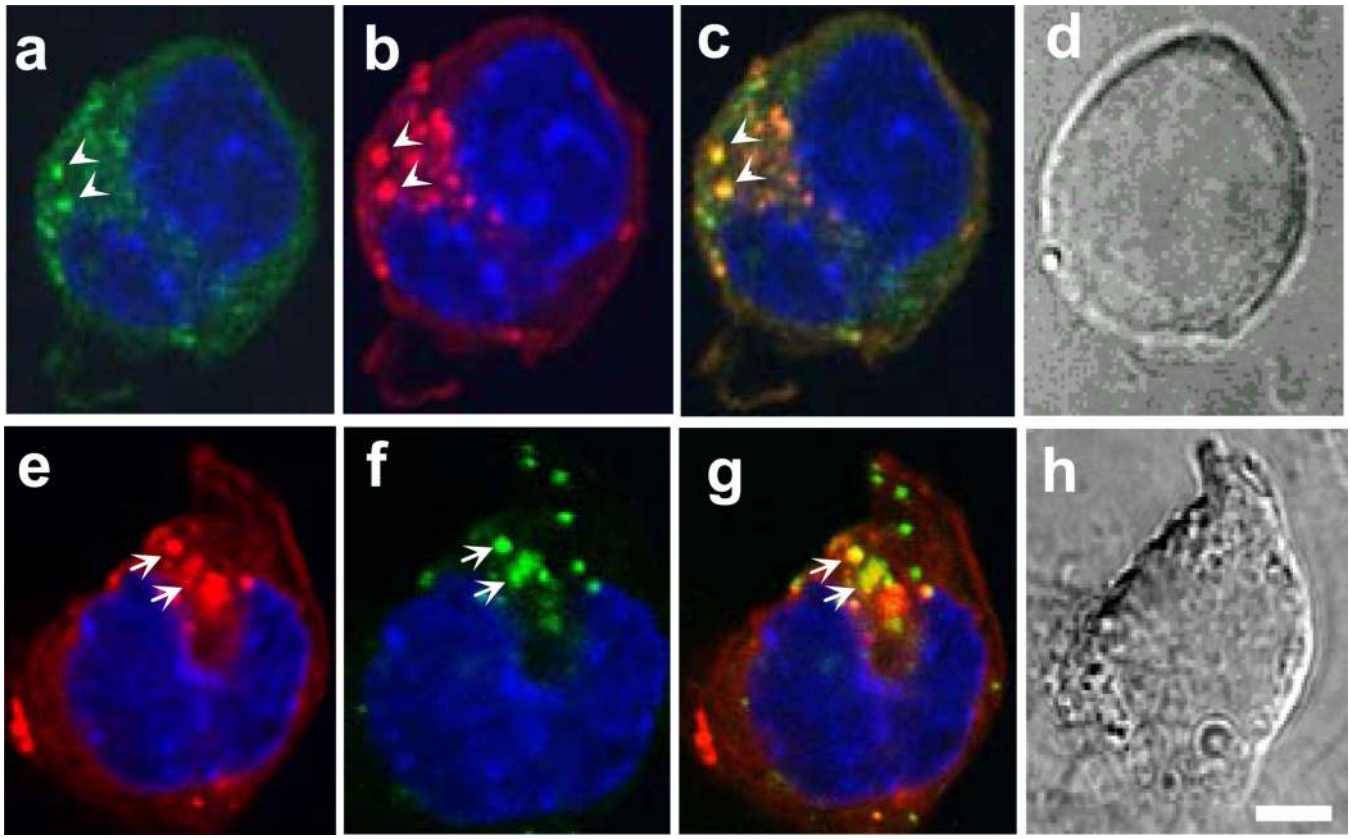

Fig. 2. LBPA and N-Rh-PE decorate MVBs from N2a cells containing IDE

Live immunofluorescence of N2a cells showing: **a**. MVBs specifically labeled with the anti-LBPA (green) and **b**. positive for the fluorescent lipid analog N-Rh-PE (red). **e**. MVBs positive for the fluorescent lipid analog N-Rh-PE (red) and f, **s**pecifically labeled with anti-IDE 1C1/3A2 monoclonal antibodies (green). Merge, **c**. Co-localization of LBPA with N-Rh-PE (arrowheads) and **g**, co-localization N-Rh-PE and IDE (arrows). Nuclei (blue) were stained with Hoesch 33342. **d** and **h**. Contrast phase microphotographs show cellular integrity. Bar size= 5μm.

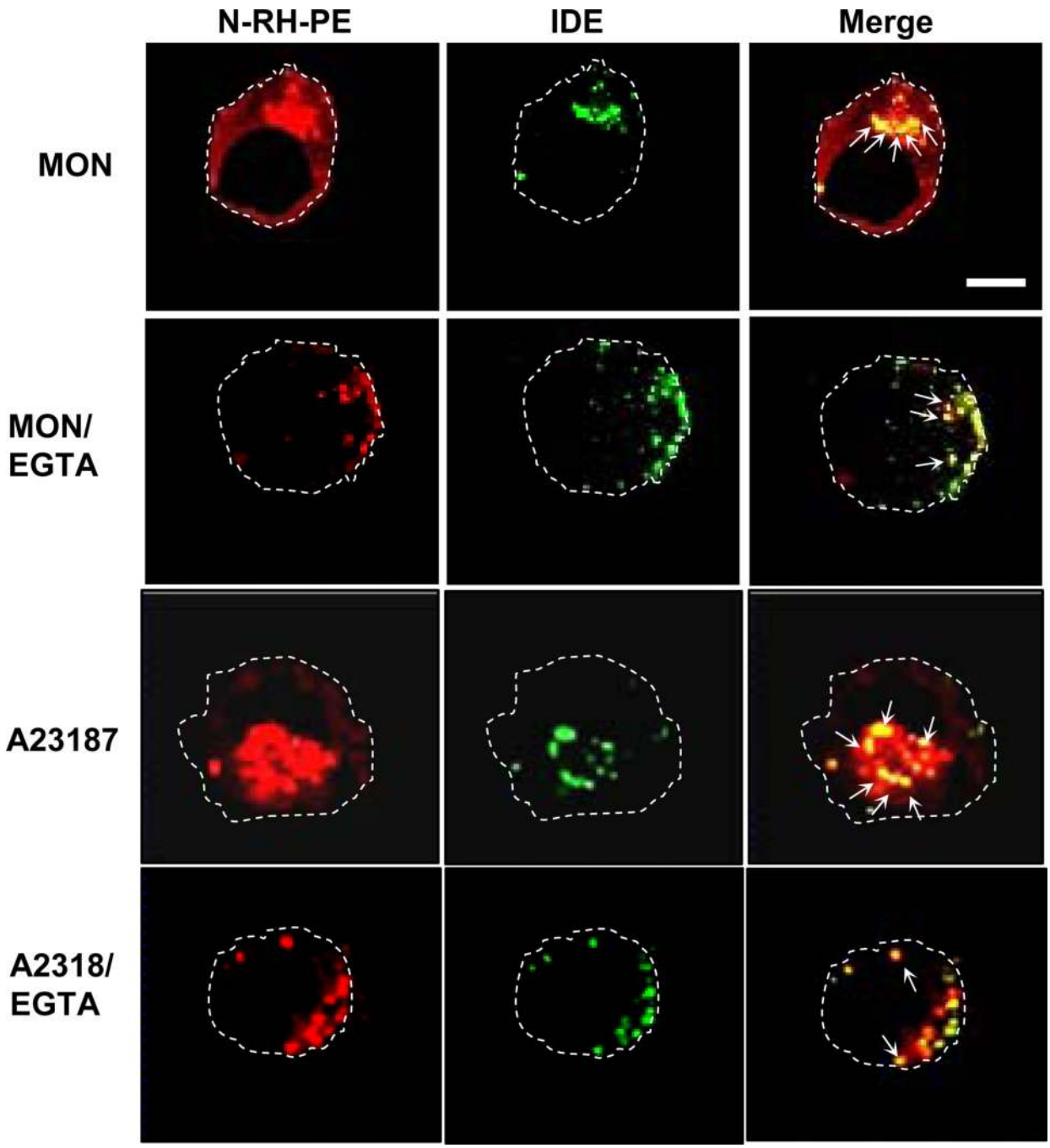

Fig. 3. Monensin and calcium ionophore induce the formation of large MVBs containing IDE

Live immunofluorescence of N2a cells showing MVBs specifically labeled with the fluorescent lipid analog N-Rh-PE (red) and anti-IDE 1C1/3A2 monoclonal antibodies (green) in cells treated with 7 μM MON; 7 μM MON/1.5 mM EGTA; 1 μM A23187 or 1 μM A23187/1.5 mM EGTA, respectively. Merge, show co-localization of IDE with MVBs (arrows). White broken line delineates the borders of the cells. Bar size= 5μm.

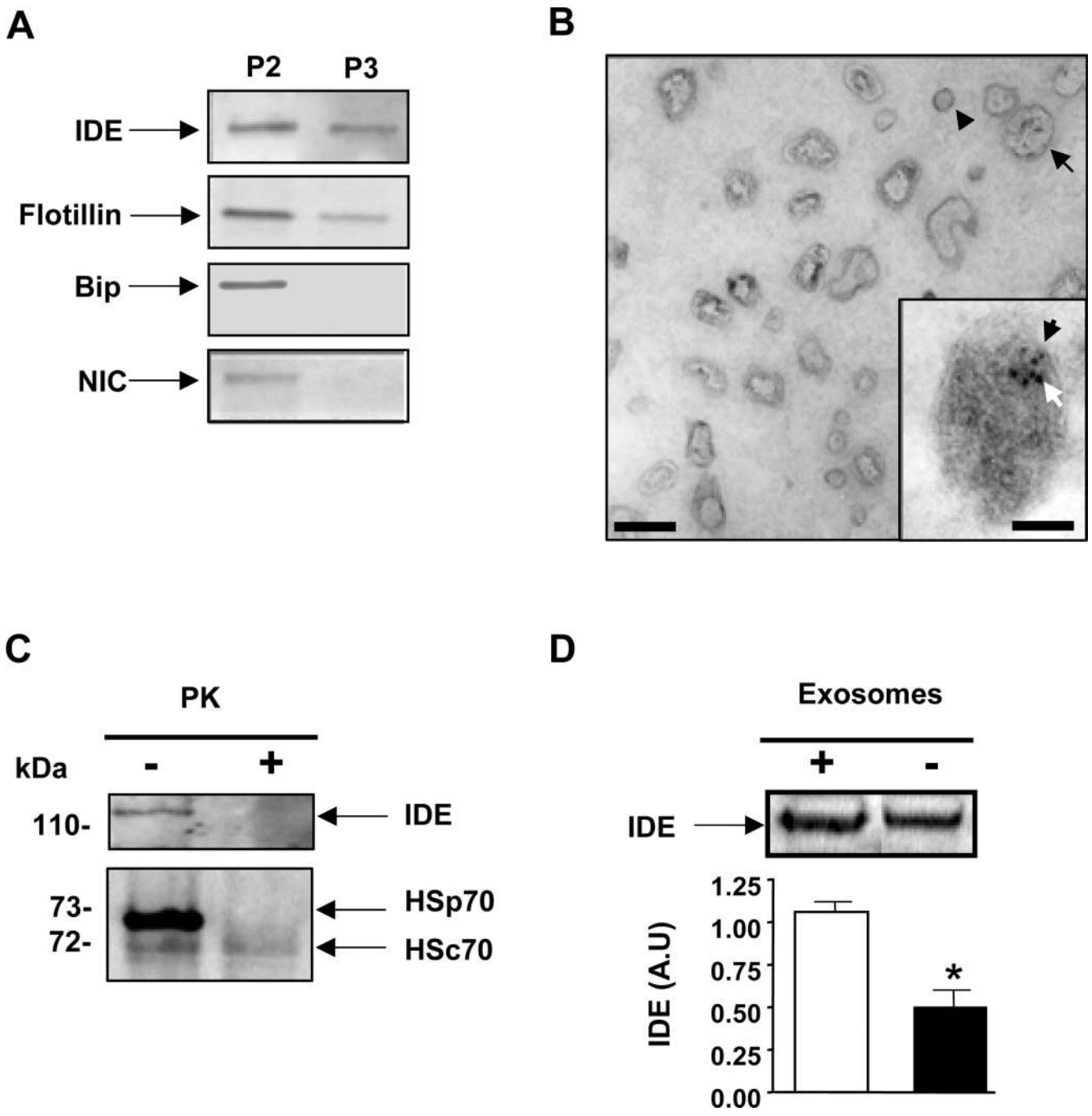

Fig. 4. IDE is released in association with exosomes

A. Representative Western blot of IDE, flotillin, Bip and NIC, respectively, of membrane pellets from differential centrifugation of N2a supernatant. P2= pellet after 12,000 xg; P3= pellet after 100,000 xg. Same amount of protein was loaded in each well. **B**. Electron-microscopic observation of whole-mounted exosomes purified from N2a cells. Arrows indicate exosomes, arrowheads point to smaller non-exosomal vesicles. Scale bar, 100 nm. Inset: Immunogold showing co-localization of TfR (15-nm gold particles) and IDE (6-nm gold particles). Scale bar, 50 nm. **C**. Representative Western blot showing IDE and Hsp/

Hsc70 immunoreactivity in purified exosomes subjected (+) or not (−) to Proteinase K (PK) limited proteolysis. **D**. Upper panel, representative Western blot showing IDE immunoreactivity after specific immunoprecipitation from N2aSW culture media untreated (+) or exosome-depleted (−). Bars show semi-quantitative analysis of IDE levels expressed in arbitrary units (A.U.) in untreated (+) compared to exosomes-depleted (−) supernatants. (1.06 ± 0.06 vs. 0.5 ± 0.1; n=3; *$p<0.05$).

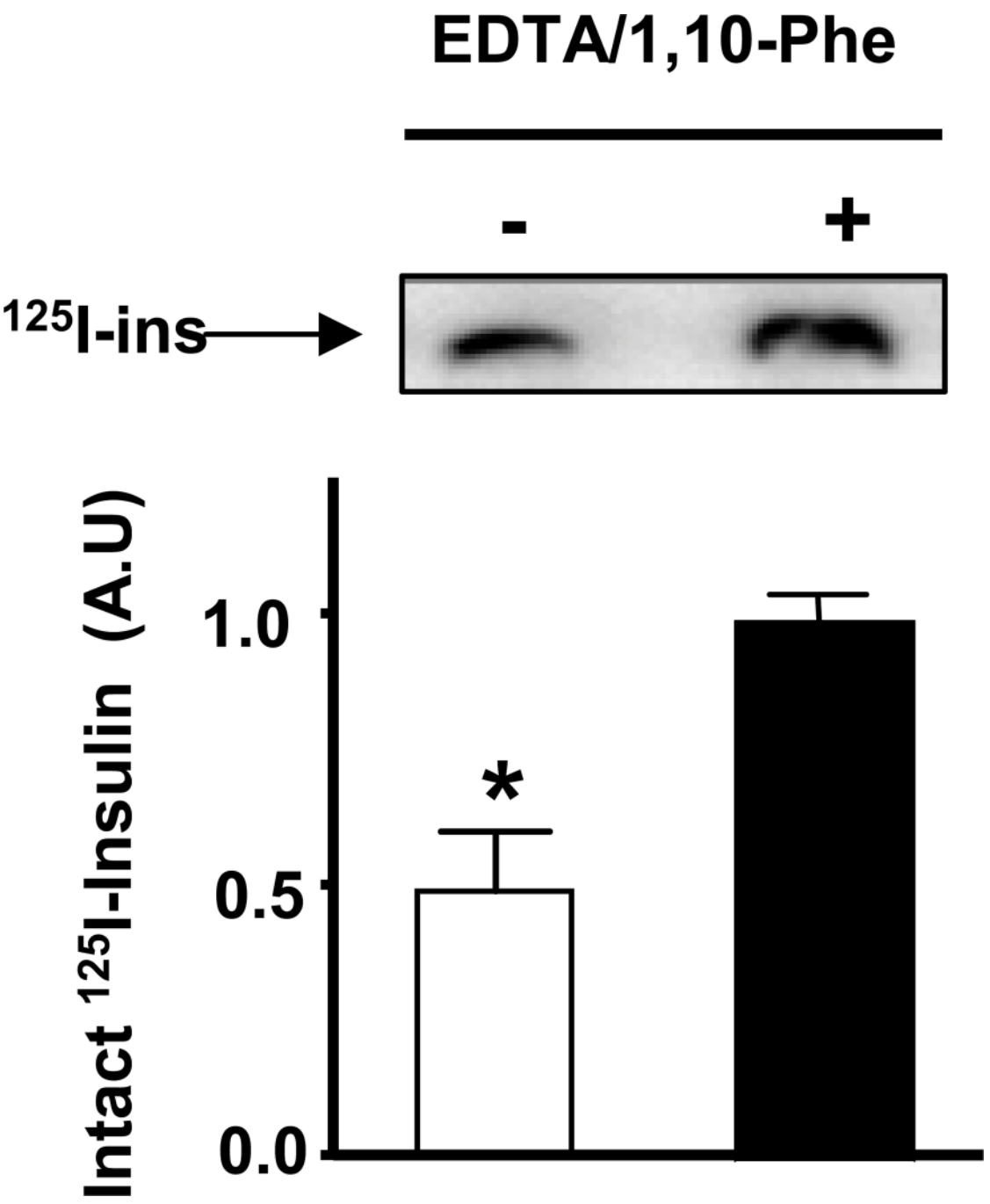

Fig. 5. Exosomes-associated IDE is proteolytically active

Exosomes were resuspended and sonicated in degradation buffer containing protease inhibitors PMSF, leupeptin, pepstatin, aprotinin, thiorphan and phosphoramidon with or without EDTA (5 mM) and 1,10-phenanthroline (1 mM). Homogenates were incubated with 35.000 cpm of ^{125}I-insulin for 3 hours and degradation was analyzed by SDS-PAGE followed by PhosphorImager quantitation. Upper panel, representative phosphorimage of insulin degradation mediated by exosomal IDE. Lower panel, semi-quantitative analysis of

insulin degradation expressed in arbitrary units (A.U.) in the presence (+) or absence (−) of EDTA/1,10 Phe (0.5 ± 0.1 vs. 1 ± 0.05; n=3; *p<0.05).

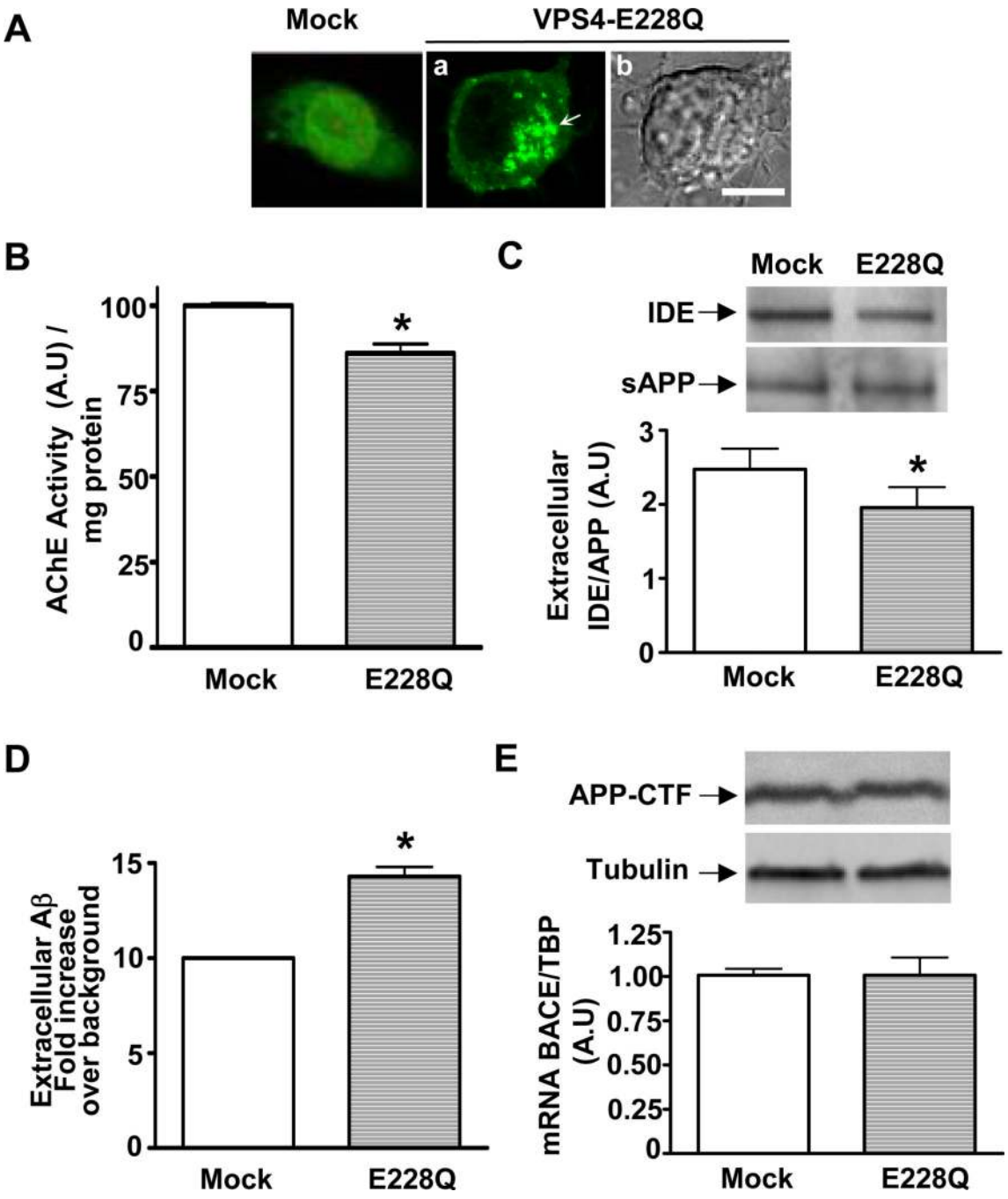

Fig. 6. VPS4 modulates the exosomal pathway, IDE release and the catabolism of endogenous Aβ

A. N2aSW cells transiently transfected with the empty vector pEGFP (mock) or pEGFP-VPS4-E228Q (VPS4-E228Q), respectively, show the characteristic cellular expression pattern. Panel **a**, arrows indicate MVBs structures significantly enlarged in VPS4-E228Q. Panel **b**, contrast phase microphotograph shows integrity of the cell depicted in panel **a**. Bar size= 5μm. **B**. Exosomes isolated from VPS4-E228Q transfected cells show a significant decrement in AChE activity as compared to mock transfected cells (100.0 ± 0.58 vs. 86.10 ± 2.70; n=3; *p<0.05). **C**. Upper panel, representative phosphorimage of extracellular IDE and

sAPP immunoprecipitated from conditionated supernatants of mock and VPS4-E228Q transfected cells. Lower panel, semi-quantitative analysis of extracellular IDE/sAPP expressed in arbitrary units (A.U.). Bars show a significant decrement in VPS4-E228Q as compared to mock transfected cells (1.95 ± 0.27 vs. 2.47 ± 0.28; n=3, *p<0.05). **D**. Bars represent the fold increase over background of extracellular Aβ levels from mock and VPS4-E228Q N2aSW transfected cells (n=3). **E**. Upper panel, representative western blot of APP-CTF and tubulin expression. Lower panel, similar levels of BACE mRNA transcripts were detected in mock and VPS4-E228Q N2aSW transfected cells (1.007 ± 0.04 vs. 1.008 ± 0.01; n=3, p=0.99).

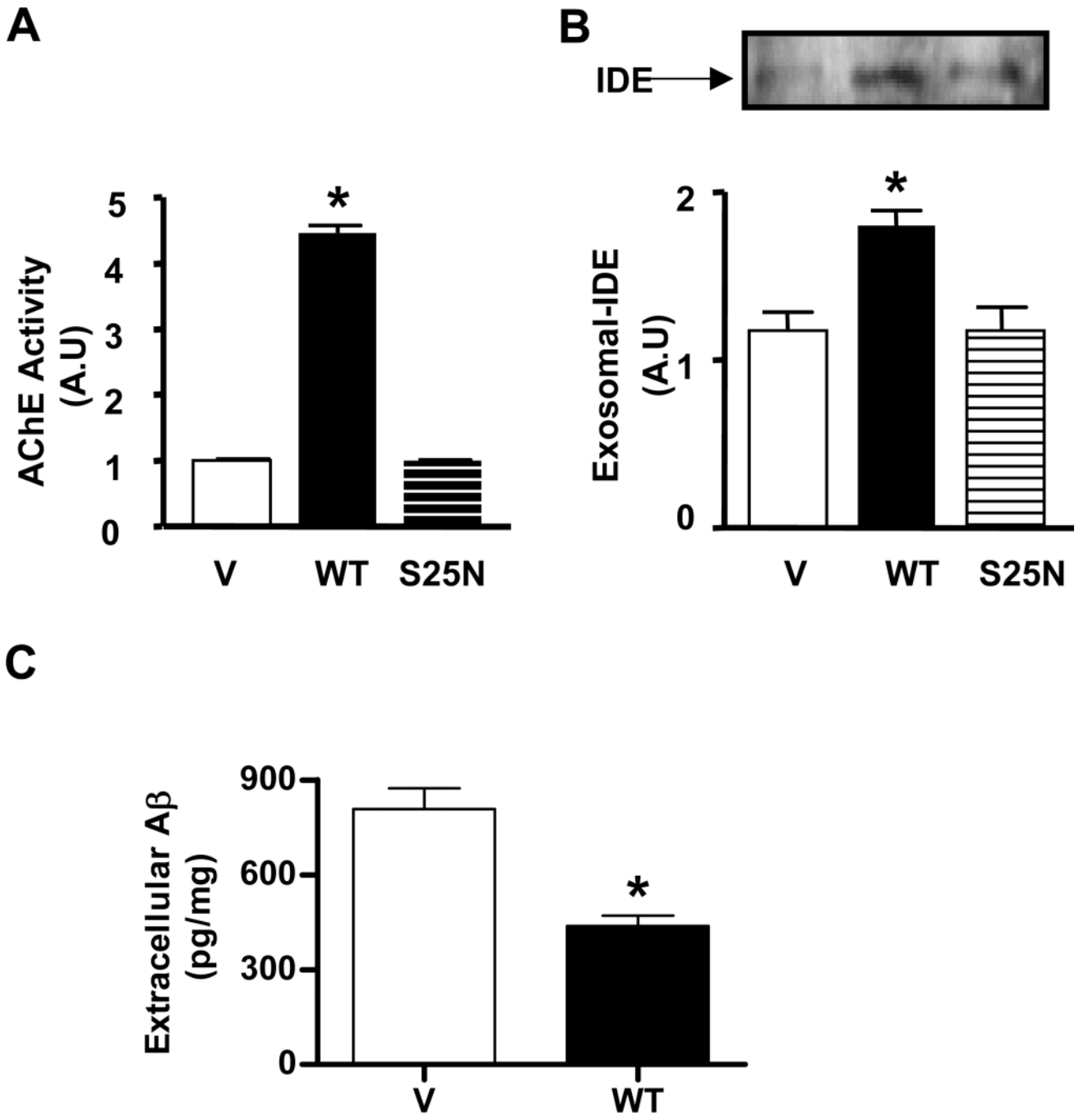

Fig. 7. Rab 11 modulates the exosome pathway and IDE release

A. Exosomes isolated from Rab11WT (WT) transfected cells show significant increments in AChE activity as compared to p-EGFP (V) control cells (4.5 ± 0.10 vs. 1.0 ± 0.05; n=2; *p<0.05) while no significant differences were obtained between control and Rab11S25N (S25N) transfected cells (1.0 ± 0.05 vs. 0.90 ± 0.01). **B**. Increments in the amount of exosome in Rab11WT (WT) were in accordance with increased exosomal-IDE levels as compared to p-EGFP control (V) (1.8 ± 0.1 vs. 1.2 ± 0.1; n=2; *p<0.05) while no differences were detected between exosomal-IDE levels from Rab11S25N (S25N) and

control cells (V) (1.0 ± 0.05 vs. 1.2 ± 0.1). **C**. Bars represent the mean ± S.E.M. of extracellular Aβ in p-EGFP (V) N2a control cells as compared to Rab11WT (WT) transfected cells (437.68 ± 32.94 pg/mg total protein vs. 807.86 ± 66.23 pg/mg total; n=3, *p<0.05).

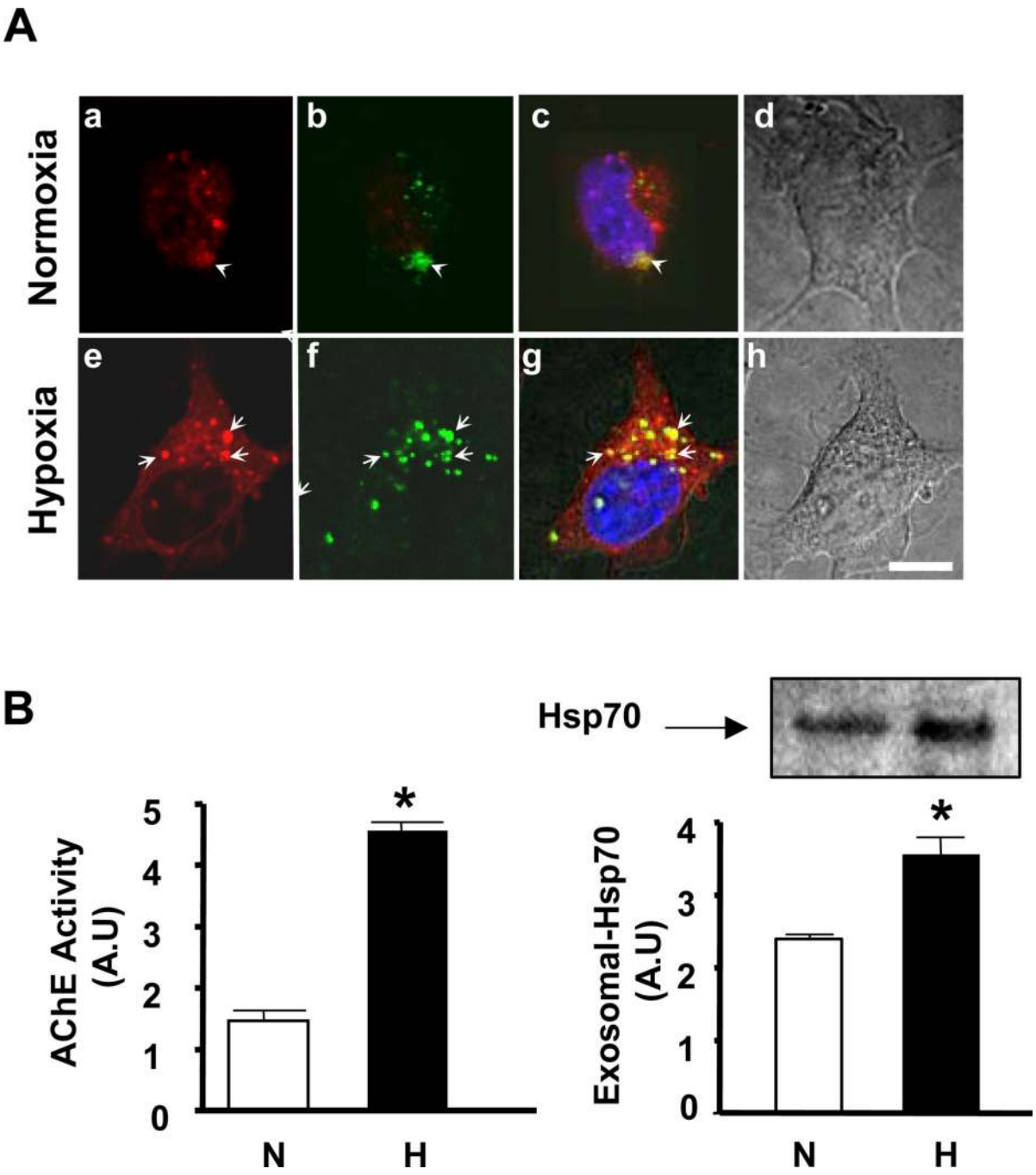

Fig. 8. Hypoxia stimulates enlargement of MVBs containing IDE and exosomal release

A. N2aSW cells were subjected to normoxia (panels a–d) and hypoxia (panels e–h) followed by MVBs (red) (panels a and e) and IDE (green) (panels b and f) labeling. Significant increment in the size MVBs (arrows) containing IDE was detected in hypoxia as compared to normoxia (arrowheads) (size particle 9.9 ± 0.9 vs. 4.6 ± 0.3 pixels/particle; n= 18 cells, $p<0.05$). Merge (panels c and d), indicate co-localization of IDE and MVBs. Nuclei (blue) were stained with Hoesch 33342. Contrast phase microphotographs show cellular integrity. Bar size= 5μm. **B**. Exosomes isolated from N2aSW hypoxic cells (H) show increased AChE

activity (left panel) (4.6 ± 0.1 vs. 1.5 ± 0.2; n=4; *p<0.001) and Hsp70 immunoreactivity (right panel) (3.5 ± 0.2 vs. 2.4 ± 0.05; n=3, *p<0.05) as compared to normoxic cells (N).

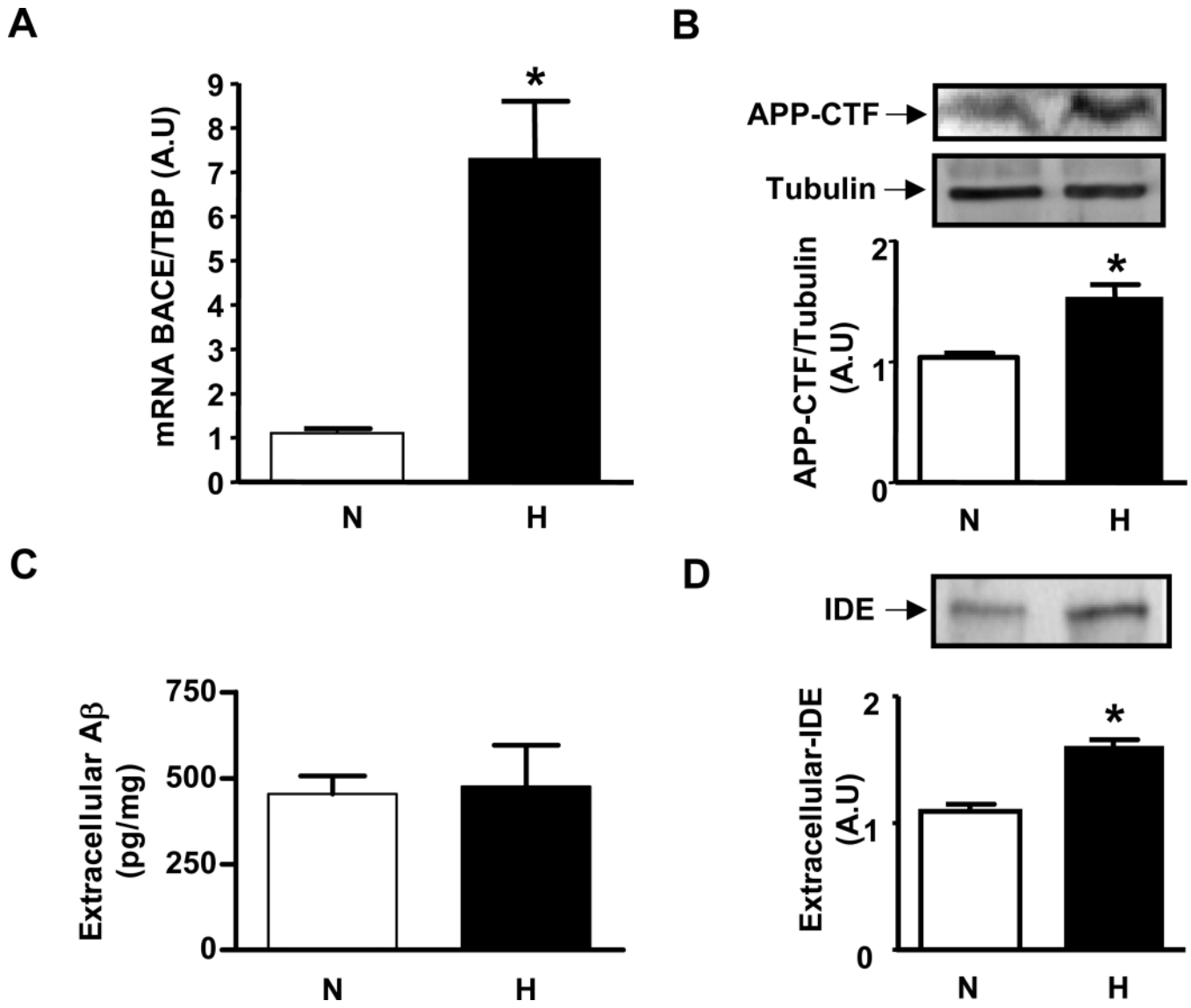

Fig. 9. Hypoxia stimulates BACE transcription, APP-CTF generation and IDE release

A. BACE mRNA levels in N2aSW cells are increased in hypoxia (H) as compared to normoxia (N) (7.3 ± 1.3 vs 1.1 ± 0.1.; n=2, * $p<0.05$). **B**. Upper panel, representative western blot of APP-CTF and tubulin expression. Lower panel, semi-quantitative analysis of APP-CTF/tubulin immunoreactivity expressed in arbitrary units (A.U.). Bars show significant increments in H as compared to N (1.53 ± 0.1 vs. 1.03 ± 0.03; n=2, *$p<0.05$). **C**. Bars represent the mean ± S.E.M. of extracellular Aβ in hypoxia as compared to normoxia (475.01 ± 120.28 pg/mg total protein vs. 454.42 ± 52.03 pg/mg total; n=4, p=0.88). **D**. Upper panel, representative phosphorimage of extracellular IDE immunoprecipitated from condionated supernatants of normoxic (N) and hypoxic (H) cells. Lower panel, semi-quantitative analysis of extracellular IDE expressed in arbitrary units (A.U.). Bars show significant increments in H as compared to N (1.8 ± 0.03 vs. 1.07 ± 0.04; n=3, * $p<0.05$).